Chemical Engineering Journal 155 (2009) 339–346

Contents lists available at ScienceDirect

Chemical Engineering Journal

journal homepage: www.elsevier.com/locate/cej

Graphite-supported TiO_2 for 4-nitrophenol degradation in a photoelectrocatalytic reactor

Giovanni Palmisano[a,b,c,*], Vittorio Loddo[a], Hossam Hamed El Nazer[a,d], Sedat Yurdakal[a,e], Vincenzo Augugliaro[a,**], Rosaria Ciriminna[b], Mario Pagliaro[b]

[a] "Schiavello-Grillone" Photocatalysis Group, Dipartimento di Ingegneria Chimica dei Processi e dei Materiali, Università degli Studi di Palermo, Viale delle Scienze, 90128, Palermo, Italy
[b] Istituto per lo Studio dei Materiali Nanostrutturati, CNR, Via Ugo La Malfa 153, 90146, Palermo, Italy
[c] Dipartimento di Ingegneria Elettronica, Università degli Studi di Roma "Tor Vergata", Via del Politecnico, 1, 00133, Roma, Italy
[d] Photochemistry Department, National Research Centre, Al-Behoos St. (El-Tahrir street), 12622 Dokki-Cairo, Egypt
[e] Kimya Bölümü, Fen Fakültesi, Anadolu Üniversitesi, Yunus Emre Kampüsü, 26470 Eskişehir, Turkey

ARTICLE INFO

Article history:
Received 20 April 2009
Received in revised form 2 July 2009
Accepted 4 July 2009

Keywords:
Photoeletrocatalytic degradation
Photoelectrocatalytic reactor
Graphite-supported TiO_2
4-Nitrophenol oxidation

ABSTRACT

Amorphous TiO_2, prepared at room temperature through a sol–gel method implementing hydrolysis of $TiCl_4$, has been supported on graphite rods and then annealed at 673 K. In this way graphite was completely covered by a porous anatase TiO_2 layer, with an external thickness of about 1 μm, with graphite pores completely filled by the semiconductor particles. The obtained electrode was structurally characterized by SEM microscopy coupled to EDAX mapping and by Raman spectroscopy. A Pyrex annular reactor was designed in order to test the prepared electrodes for the photoelectrocatalytic degradation of 4-nitrophenol, a target pollutant dissolved in aqueous conductive solution. The continuous reactor worked in total recirculation mode and the degradation runs were carried out by applying near UV-light, bias or both energy sources. The influence of flow rate, initial 4-nitrophenol concentration and applied potential on the degradation rate was studied.

© 2009 Elsevier B.V. All rights reserved.

1. Introduction

The efficiency of heterogeneous photocatalytic processes carried out through semiconductor oxides is measured through the quantum yield which is defined as the number of molecules reacting per absorbed photons. It is very difficult to measure the actual absorbed light in heterogeneous systems due to scattering of light by the semiconductor particles. The common approach is to assume that the entire incident light is absorbed and in this case the efficiency is quoted as an apparent quantum yield. The charge recombination between the photogenerated electrons and holes is the main factor lowering the quantum yields of the reactions. In fact, in competition with charge transfer to adsorbed species, there is the electron–hole recombination [1–4], that can occur in the bulk or on the surface of the semiconductor particle with the release of heat. Without recombination the quantum yield of the photocatalytic process would assume the ideal value of 1. In this case the rate of charge transfer would be dependent on the diffusion of charge carriers to the surface in the absence of excess surface charge. This case is an idealization; in a real system recombination does occur and the concentration of electrons and holes at the surface is not equal.

Electron and hole recombination is eventually detrimental to the efficiency of a semiconductor photocatalyst so that many efforts have been made for its enhancement such as by means of doping with metal, non metal and ions. The efficiency of photocatalytic processes may be improved by electrochemical means [5–17]. This technique combines UV illumination with the application of a controlled potential through a supported catalyst, resulting in a decrease in the recombination rate of photogenerated electrons and holes. In fact under the applied external anodic bias the photogenerated electrons are quickly driven to the counter electrode through external circuit whereas the photogenerated holes react with surface hydroxyls or adsorbed water to generate some reactive species, such as •OH; by forcing the photogenerated electrons and holes in different directions, the charge recombination is reduced to a large extent.

The combination of heterogeneous photocatalysis with external electric field appears to be one of the most promising ways for improving the performances of photocatalytic oxidations. This improvement is strictly related to the determination of the optimum value of applied voltage for which the oxidation process exhibits the highest performance at the lowest cost.

* Corresponding author. Tel.: +39 091 23863720; fax: +39 091 7025020.
** Corresponding author.
E-mail addresses: gpalmisano@dicpm.unipa.it (G. Palmisano), augugliaro@dicpm.unipa.it (V. Augugliaro).

1385-8947/$ – see front matter © 2009 Elsevier B.V. All rights reserved.
doi:10.1016/j.cej.2009.07.002

Slurry photoelectrocatalytic reactors have been tested and the influence of cell voltage, treatment time, oxygen concentration, pH value, catalyst amount and the conductivity of solution on the process were investigated [11]. Film photoanodes have been also prepared and tested. The photoelectrocatalytic oxidation of aniline was performed both in single and double compartment photoreactors by using TiO_2 film photoanodes prepared by direct oxidation of titanium sheets in furnace under an atmosphere of air [18]. The kinetics and mechanism of photoelectrocatalytic oxidation of nitrite ion by using the rutile form of a TiO_2/Ti photoelectrode with high electric field enhancement were also investigated [19].

Solar photoelectrochemical reactors have been also developed [20]. Large reactors of various sizes were employed containing cylindrical photoanodes surrounding the counter electrode compartment; the electrodes were placed inside the glass tubes of either compound parabolic or parabolic trough collectors. In particular the degradation of model pollutants at various solar light intensities has been performed. Ti/TiO_2 photoanodes have been prepared from large cylindrical Ti metal foils. A thin (100 nm) TiO_2 film was deposited on these cylindrical Ti sheets by dipping them into a methanol colloidal suspension containing TiO_2 particles (20 nm in size) [14].

This paper reports the results of an investigation devoted to the preparation and characterization of TiO_2-coated graphite rods, used as photoanodes for the oxidation of 4-nitrophenol (4-NP) in a continuous reactor. During industrial manufacturing and processing huge amounts of different organic substances, including nitrophenolic compounds, enter the environment. An important member of this group is 4-NP, which is applied in agriculture, dyes/pigments, engineering polymers, and pharmaceuticals [21]. Owing to its significant solubility in water, 4-NP breaks down readily in surface waters, but it takes a long time to degrade in deep soil and ground water, being toxic to plant, animal and human health. In view of its toxic effects, efforts have been made to remove it from wastewater. The 4-NP photocatalytic degradation in aqueous TiO_2 suspensions has been widely studied [22–24]; the main reaction intermediates have been identified [25] and the possible reaction pathways have been also investigated [26]. From the observed formation of hydroxynitrobenzene isomers there is a general agreement that the major reaction pathway in the 4-NP photocatalytic degradation involves the hydroxyl radicals generated onto the catalyst surface by irradiation.

Electrocatalytic systems have been tested for 4-NP degradation [27,28]; the main intermediates detected were 4-nitrocatechol, 2-hydroxy-benzoquinone, hydroquinone and benzoquinone. It is generally accepted that, when the current is switched on, numerous hydroxyl radicals are formed. These hydroxyl radicals react with 4-NP mainly through electrophilic addition with the C–C double bonds of the benzene ring to form initially substituted aromatic products.

Photoelectrocatalytic degradation of 4-NP [29,30] has been performed in batch cell and investigated from kinetic and mechanistic points of view. The use of hydrodynamic differential pulse voltammetry technique [31] to a TiO_2 rotating disk electrode allowed to determine that hydroquinone, the main electroactive intermediate product of 4-NP degradation, was produced through the direct reaction between the highly powerful oxidant $^{\bullet}OH$ radical and 4-NP. Therefore it is accepted that the degradation mechanism of 4-NP by photoelectrocatalytic oxidation over TiO_2 involves the generation and reaction with $^{\bullet}OH$ radicals as in the photocatalytic processes. The applied cell voltage accelerates the degradation of 4-NP by reducing the electron–hole recombination but it does not change the degradation mechanism of 4-NP.

In the present investigation the degradation tests of 4-NP aqueous solutions were carried out by using a continuous annular photoelectrocatalytic reactor with total recirculation of reacting electrolyte solution. The photoanodes were home prepared by supporting TiO_2 onto graphite rods. Graphite was selected as support anode due to its low cost and high conductivity, in contrast with the common approach making use of titanium. The obtained electrode was analysed by means of SEM coupled to EDAX mapping, in order to study the electrode surface morphology and the cross-sectional distribution of TiO_2. Raman spectroscopy has been used in order to investigate TiO_2 crystallinity.

2. Experimental

2.1. Reactor

The set up used for all the reactivity runs is reported in Fig. 1; it consisted of a photoelectrocatalytic reactor (PECR) in a recirculation loop with a well stirred tank (ST) in which the oxygenation of electrolyte solution was carried out by a continuous bubbling of pure oxygen. The Pyrex annular PECR (outer diameter: 7.0 cm; annulus gap: 1.5 cm and height: 10.0 cm) was specifically designed and constructed; its scheme is reported in Fig. 2. Graphite rods (purchased from Sigma–Aldrich: diameter: 3 mm; length: 15 cm) played the role of anodes, whereas a gold sheet was the cathode. A 125 W medium pressure Hg lamp (Helios Italquartz, Italy) was positioned in the axis of the photoreactor; it was cooled by water circulating through a Pyrex thimble. The radiation energy entering in the reacting volume from the inner surface of annulus had an average value of 10 mW cm^{-2}. It was measured by using a radiometer UVX Digital, at $\lambda = 360$ nm. The six anodes were placed axially with respect to the lamp whereas the golden sheet cathode covered all the inner surface of the outer annulus tube for a height of 12 cm; in this way the cathode also worked as a reflecting surfaces allowing the irradiation of the rear part of anodes. The total geometric surface of anodes exposed to light was ca. 56 cm^2.

Fig. 3 shows the Teflon support used to maintain at a fixed position the upper part of anodes. Two series of holes are present: the small internal ones provide the place for graphite rods, whereas the bigger ones allow an easy circulation of electrolyte. The space of the annulus between the cathode and the anodes was filled with beads of 3 mm diameter, in order to minimize the residence time of electrolyte inside the reactor; the beads were of Pyrex glass so that they did not absorb any fraction of the UV-radiation entering the photoreactor. The total liquid hold up inside the reactor, V_{PECR}, was 130 mL. A peristaltic pump was used to feed the O_2-saturated aqueous solution to the bottom of the reactor at a constant flow rate. A potentiostat (CHI630B Electrochemical Workstation, CH Instruments) was connected to anodes and cathode.

2.2. Photoanode preparation and characterization

Graphite rods were purchased from Sigma–Aldrich; before supporting TiO_2, they were immersed in NaOH 10 M aqueous solution for 30 min. Afterwards the rods were ultrasonicated in distilled water for 1 h in order to clean them and to obtain a uniform surface; the cleaning procedure was repeated three times.

Titanium tetrachloride (Fluka 98%) was used as starting material for the preparation of TiO_2 supported over graphite. $TiCl_4$, without any preliminary purification, was slowly added to distilled water (volume ratio: 1:10) at room temperature. The hydrolysis reaction was highly exothermic and produced a certain amount of HCl fumes. After ca. 10 h of continuous stirring at room temperature, a clear solution was obtained. The graphite rods were immersed and kept inside the clear solution for 1 h. Thereafter the graphite rods were dried at 343 K for ca. 20 min and then calcined in air at 673 K for 3 h. This procedure, repeated 10 times, gave rise to stable pure anatase films over graphite. The crystalline phase was

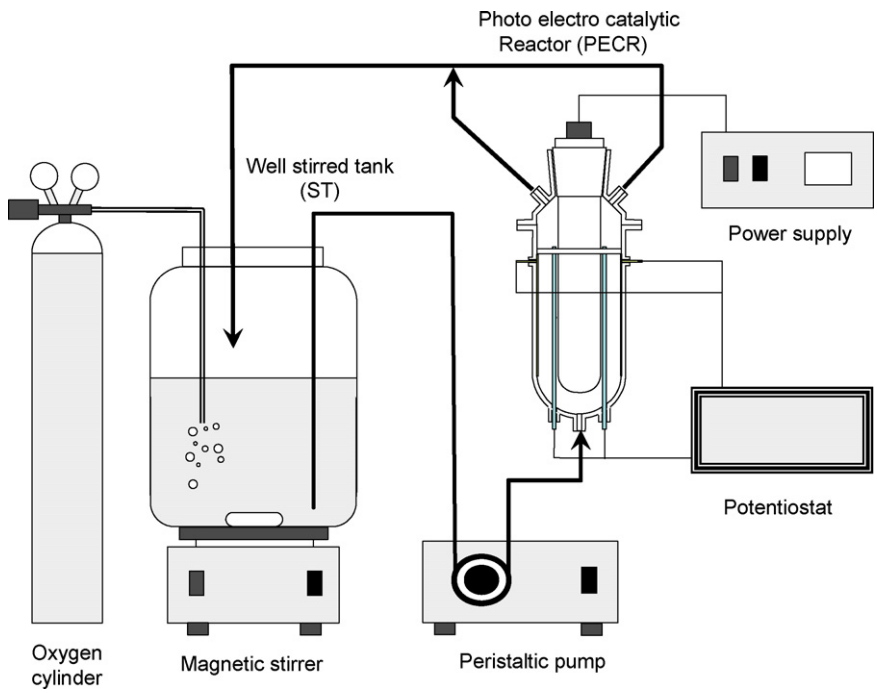

Fig. 1. Set up of experimental apparatus.

detected through Raman spectroscopy. A microprobe set-up (ISA-Jobin-Yvon, model Labram), equipped with a CCD detector and a He–Ne laser as excitation source (632.8 nm emission), was indeed used. SEM images, obtained using a microscope (Philips XL30 ESEM) operating at 25 kV and coupled to EDAX analyses, were recorded to monitor the surface morphology, and EDAX mapping was used in order to determine the cross-sectional distribution of TiO_2. The samples to analyse rod cross-sectional surface were prepared by freezing a graphite rod in liquid nitrogen and then breaking it through brittle fractures.

2.3. Reactivity runs procedure and analytical methods

The aqueous solution used to perform photo-, electro- and photoelectro-catalytic runs contained 4-NP (7.2×10^{-2} mM) and Na_2SO_4 (2×10^{-2} M) in order to ensure solution conductivity. In some runs 4-NP initial concentration was moreover ranged between ca. 2×10^{-2} and 1.5×10^{-1} mM in order to study the influence of substrate concentration on the reacting system. Positive biases were applied, by using the functionalized graphite rods always as anodes. Before all the runs, the whole aqueous solution (total liquid volume, $V_T = 0.5$ L) was put in the stirred tank (ST) and O_2-saturated by bubbling pure oxygen; this bubbling was maintained during all the reactivity runs, that lasted 6 h. After 30 min bubbling and circulating the liquid in the reactor through a peristaltic pump, in order to saturate the suspension and to reach the adsorption/desorption equilibrium, the reaction started by turning the lamp on and/or applying the bias. That time was taken as the zero time of the run. Liquid samples were withdrawn at fixed intervals of time at the inlet of reactor and analyzed by means of a Beckman Coulter HPLC (System Gold 126 Solvent Module and 168 Diode Array Detector), equipped with a Luna 5 μ phenyl–hexyl column (250 mm long × 2 mm i.d.), using Sigma–Aldrich standards.

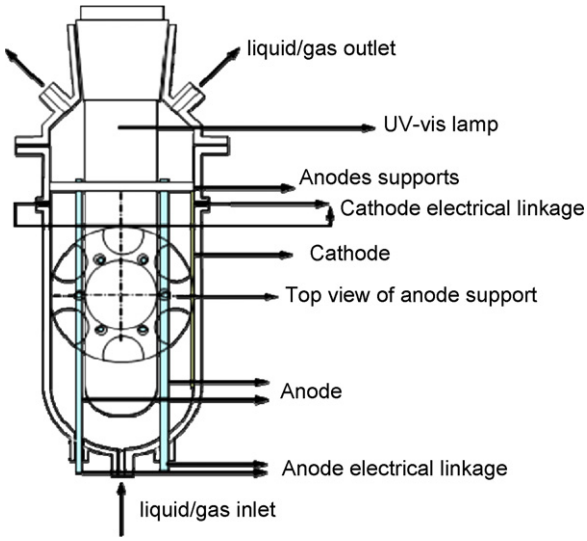

Fig. 2. Scheme of the photoelectrocatalytic reactor (PECR).

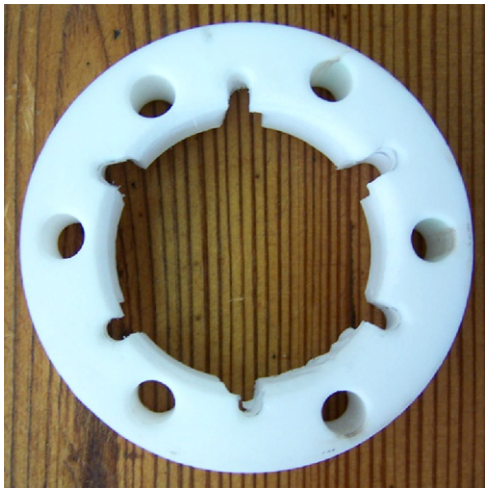

Fig. 3. Teflon support.

Retention times and UV spectra of the compounds were compared with those of standards. The eluent consisted of: 17.5% acetonitrile, 17.5% methanol, and 65% 40 mM KH_2PO_4 aqueous solution.

Since the main purpose of using the photoelectrocatalytic method is that of checking the mineralization degree of the organic compound, the monitoring of the total organic carbon (TOC) content in the course of runs was also carried out (Shimadzu 5000). The results were completely unreliable as the graphite electrodes were releasing small amounts of carbon to the solution during the runs; these very small amounts were comparable to the 4-NP carbon content. Mineralization was however checked through the use of HPLC, able to check the presence/absence of peaks at any wavelength.

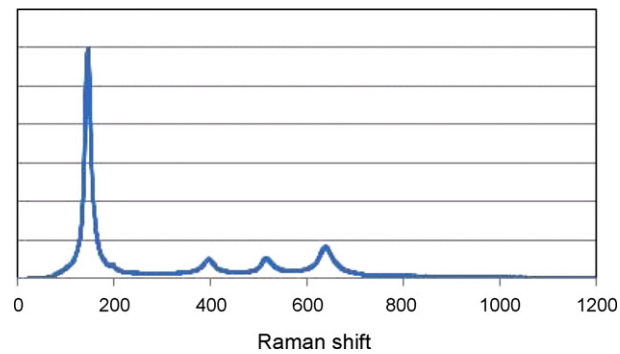

Fig. 4. Raman spectrum of a TiO_2-covered graphite rod.

3. Results and discussion

3.1. Anodes characterization

As described in the Section 2, the covering procedure of graphite rods was repeated 10 times, since depositing less layers of catalyst yielded lower photocatalytic reactivity, indicating that not all the rod surface was indeed uniformly covered. The anodes showed to be resistant to mechanical friction, stable in time (they have been used for ca. 6 months without any loss of activity), and the supported TiO_2 did not leach significantly when the graphite rods were immersed in the aqueous reacting solution.

The Raman spectra, recorded by analyzing the anodes surface and reported in Fig. 4, clearly show that the only crystalline phase present is anatase, since all the four sharp peaks (at 145, 400, 520 and 644 cm^{-1}) refer to that allotropic phase. The underlying graphite did not affect the measurement at all. The annealing temperature chose for the catalyst preparation (673 K) guarantees the absence of rutile phase. Literature reports [32–34] that pure anatase TiO_2 nanoparticles, trapped in porous silica aerogels, showed excellent photocatalytic performance being an order of magnitude more active for trichloroethylene photooxidation and six orders of magnitude greater for Bacillus subtilis cells inactivation than the commercial Degussa P25 TiO_2. On the contrary the rutile phase obtained at calcination temperatures beyond 873 K deteriorated the activity of the photoelectrocatalytic degradation of rhodamine B in water [35].

The surface of bare graphite rods, analyzed after the cleaning treatments described in the experimental part, appears really rough and irregular when observed by SEM microscopy (Fig. 5a). After functionalisation with TiO_2, however, the surface is very smooth indicating indeed that the TiO_2 sol precursor has filled all the

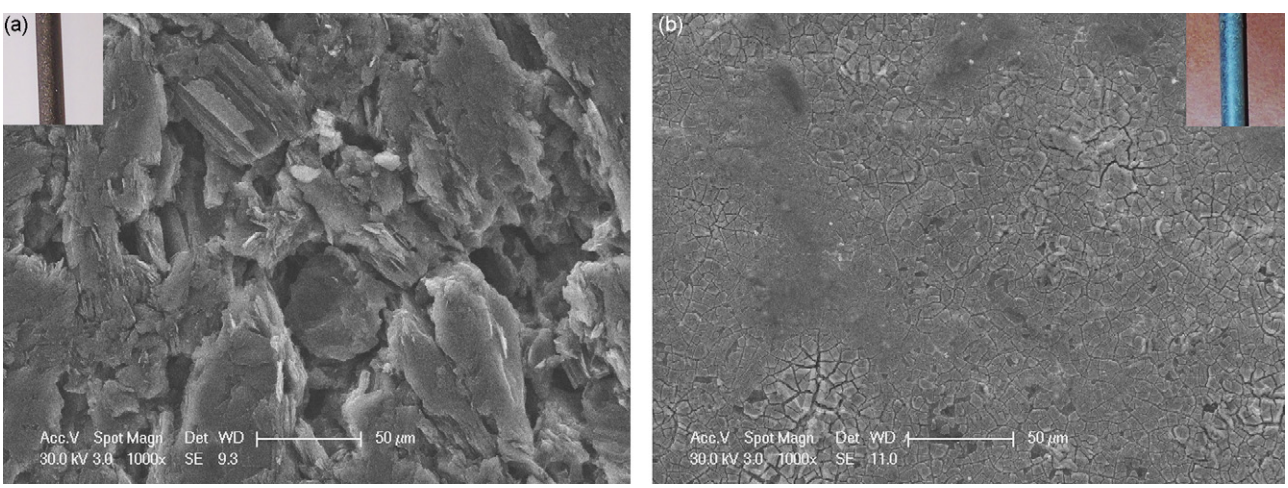

Fig. 5. SEM images and digital photos (insets) of anode's bare (a) and functionalised (b) surface.

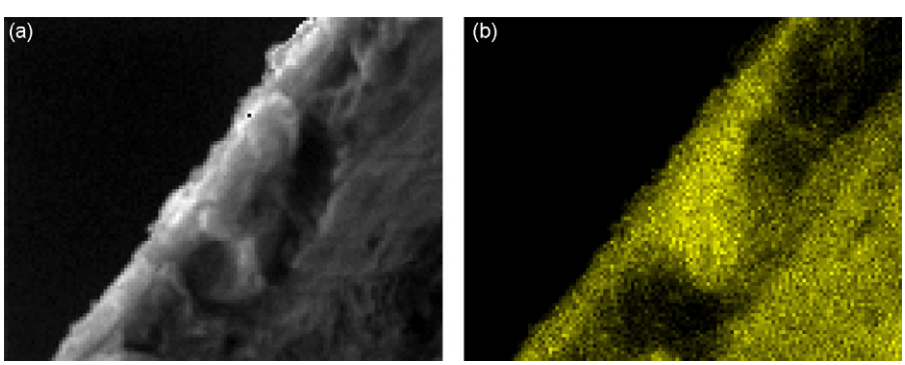

Fig. 6. Cross sectional SEM image (a) and the corresponding EDAX mapping (b) of functionalised anode. Ti is yellow-coloured.

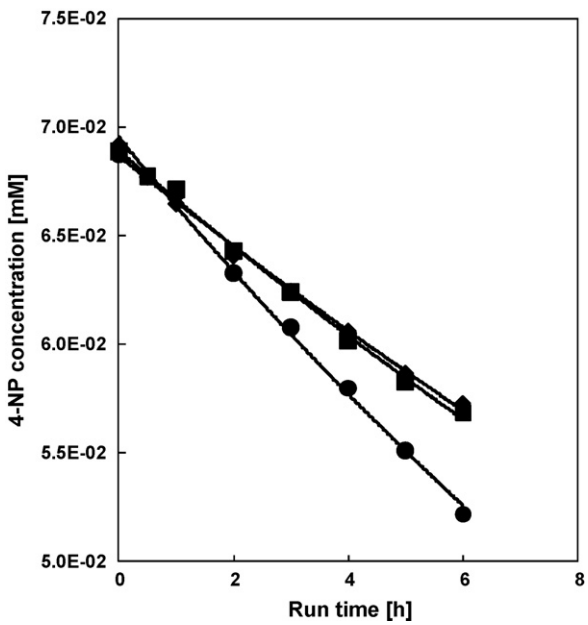

Fig. 7. 4-NP concentration values versus the run time for (♦) photocatalytic, (■) electrocatalytic and (●) photoelectrocatalytic representative runs.

graphite pores during the deposition of the first layers and then formed a uniform thin film above (Fig. 5b).

This feature was confirmed by analyzing the cross-sectional surface of the electrode by means of EDAX mapping. Fig. 6 shows a representative SEM image and the corresponding EDAX mapping made in order to identify Ti distribution. It can be seen that TiO_2 greatly enters the rod pores and that an external layer is however formed with a minimum average thickness of ca. 1 μm.

3.2. Reactivity

The photo-, electro- and photoelectro-catalytic runs always produced the same stable intermediates of 4-NP degradation, i.e. hydroquinone and 4-nitrocathecol. The carbon mass balance, carried out by taking into account the concentrations of 4-NP and stable intermediates, was satisfied for more than 97% thus suggesting that 4-NP mineralization does not occur at the used experimental conditions.

Fig. 7 reports the experimental results of 4-NP concentration values (measured at the inlet of reactor) versus the run time for three typical photo-, electro- and photoelectro-catalytic runs. Even if it is well recognized that the photoelectrocatalytic degradation of organic pollutants follows pseudo-first-order kinetics [36], different kinetics (zero and first order and Langmuir–Hinshelwood model) have been fitted to the data. Independently of the energy source, however, it was found that the 4-NP disappearance rate, ($-r_{4\text{-NP}}$), is best described for all the runs by pseudo-first order kinetics with respect to 4-NP concentration:

$$(-r_{4\text{-NP}}) = -\frac{dC}{dt} = k_{\text{app}}C \tag{1}$$

in which C is the 4-NP concentration at the inlet of reactor, t the run time and k_{app} the apparent pseudo-first order rate constant. The k_{app} kinetic constant, used in this paper to characterise the observed oxidation rates, is not a "constant" as it is affected by several key factors such as 4-NP concentration, light intensity, total irradiated area of TiO_2 electrodes, voltage of applied electrical bias, pH condition, etc. Integration of Eq. (1) with the limit condition that $C = C_0$ at $t = 0$ gives:

$$C = C_0 \exp(-k_{\text{app}}t) \tag{2}$$

By applying a least-squares best fitting procedure to the 4-NP reactivity data, Eq. (2) allows to determine the best values of k_{app}. In Fig. 7, the lines through the experimental data have been drawn by using Eq. (2); it may be noticed that a very satisfactory fitting of the model to the data occurs. For all the runs the fitting of data to Eq. (2) gave determination coefficient (R^2) values higher than 0.99 whereas for zero order kinetics the R^2 values were in the 0.96–0.99 range.

The photoreacting system used in this work (see Fig. 1) is composed by a PECR and a ST. The biased and/or irradiated PECR determines the occurrence of 4-NP degradation whereas the presence of a ST on the recycle loop determines that the 4-NP concentration at the PECR inlet is different from the outlet one. The system is not at steady state so that the PECR inlet and outlet concentrations are varying with time. The dynamics of this system has been discussed in detail by Wolfrum and Turchi [37] for a photocatalytic reaction whose kinetics obeys two limiting cases of the Langmuir–Hinshelwood rate expression, i.e. the cases for which the rate equation approaches zero order and first order. The authors [37] demonstrate that, in both the cases, provided that the value of the photoreactor residence time is small, the following relationship holds:

$$\frac{dC}{dt} = \left[\frac{V_{\text{PR}}}{V_{\text{T}}}\right] r(C) \tag{3}$$

in which V_{PR} is the liquid volume contained in the photoreactor, V_{T} the total liquid volume, C the inlet concentration to the photoreactor and $r(C)$ is the rate equation evaluated at the inlet concentration. In other words, in a recycle system with low per-pass conversion determined by low values of residence time for zero and first order kinetics, the k_{app} values, determined by means of the measured values of concentration, are underestimated. The true values of kinetic constant (k_{T}) must be obtained by dividing the k_{app} ones by the ratio of the liquid volume contained in the photoreactor to the total liquid volume. In the present case the $V_{\text{PECR}}/V_{\text{T}}$ value is 0.26 and the true kinetic constant is $k_{\text{T}} = k_{\text{app}}/0.26$. On this basis the values of k_{T} are hereafter used for comparing the performances of different reacting systems.

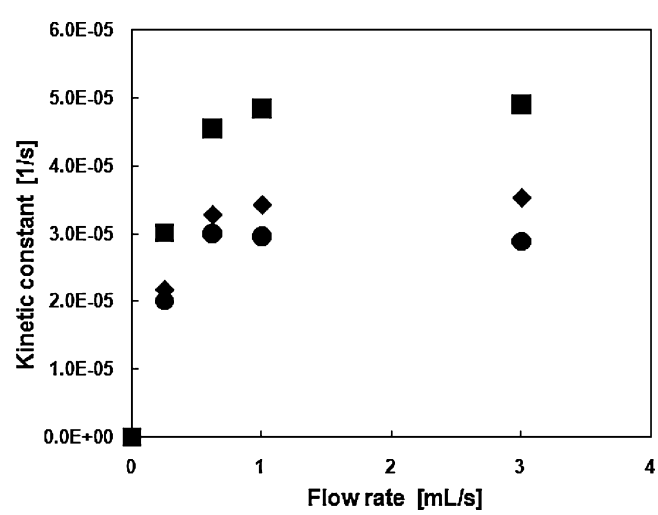

Fig. 8. Kinetic constant, k_{T}, *vs.* liquid flow rate for 4-NP photocatalytic oxidation (●), electrocatalytic oxidation with applied bias of 1 V (♦) and photoelectrocatalytic oxidation with applied bias of 1 V (■).

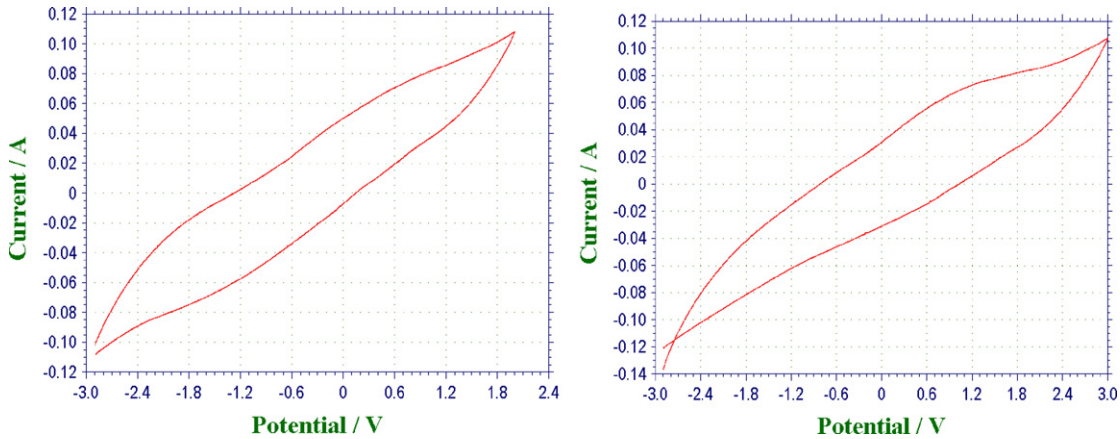

Fig. 9. Cyclic voltammetry in the absence (left) or presence (right) of light.

3.2.1. Influence of flow rate

Fig. 8 reports the k_T values obtained from photo-, electro-, and photoelectro-catalytic runs carried out at different flow rates. In the case of photocatalytic runs it can be seen that for flow rate values higher than ca. 0.6 mL/s no significant difference in k_T values is observed, thus suggesting that for that limit flow rate the mass transfer resistance plays a negligible role on the process rate. The rate limiting step hence can be assumed thus to be the substrate oxidation.

The electrocatalytic oxidation of 4-NP was carried out by selecting a bias value for which a degradation rate similar to the photocatalytic one was observed. The application of 1 V properly satisfied this condition. The values of k_T constant obtained with electrocatalytic runs also show that the limit flow rate is equal to that obtained from photocatalytic runs, i.e. ca. 0.6 mL/s.

Reactivity runs carried out with contemporary application of light and a 1 V bias showed that the limit flow rate was higher, i.e. ca. 1 mL/s. This finding can be explained by considering that the TiO_2 surface in the presence of irradiation and bias gets more reactive and therefore the mass transfer resistance plays a role even at higher flow rates.

By comparing the values of k_T constant obtained from photocatalytic, electrocatalytic and photoelectrocatalytic experiments at 1 V bias, it can be seen that the disappearance rate of 4-NP is surely higher when both energy sources are provided. The increase (from ca. 3×10^{-5} to 5×10^{-5} s^{-1}) is about 50% with respect to both photocatalytic and electrocatalytic constants.

It must be reported that, if the photoelectrocatalytic process is compared with that resulting from both the photocatalytic and electrocatalytic one, the performance of photoelectrocatalytic one results lesser than the sum of the two ones. The assumption underlying that way of comparison would be that the photocatalytic and the electrocatalytic processes can occur in parallel on the TiO_2 surface independently from the each other. In our opinion, however, this assumption does not hold in our case owing to the fact that they operate with the same mechanism, as stressed by the finding that the same intermediate products are generated by the three processes. Even if it is not correct to invoke the presence of a synergetic effect in the photoelectrocatalytic process, in our opinion the enhancement of 4-NP degradation by photocatalysis in combination with an electrical field is determined by the fact that the external electric field reduces the chances of the recombination of the electron–hole pairs.

3.2.2. Influence of electrode potential

The application of an anodic bias potential to a photoelectrode provides a potential gradient within the semiconductor film to efficiently drive away the photogenerated holes and electrons at opposite directions thus decreasing their recombination rate. In general, the higher the applied bias potential the faster the reaction is. Accordingly, the bias potential applied to the TiO_2/graphite electrode increases the number of holes available to initiate the 4-NP oxidation process.

To verify the importance of bias potential on 4-NP degradation, experiments were carried out in 4-NP solutions under different electrode potentials ranging from +1 V to +3 V. Fig. 9 reports the cyclic voltammetries for TiO_2/graphite photoelectrode in a 0.02 M Na_2SO_4 solution in the absence or presence of irradiation. At 1 V the current values are 6.7×10^{-2} A without irradiation and 8.1×10^{-2} A with irradiation. The measured difference is clearly due to the light effect.

At increasing positive potentials the 4-NP degradation rate increases. The effect of applied cell voltage is shown in Fig. 10 which reports the k_T values obtained at various biases by keeping the flow rate constant at 3 mL/s; the k_T value obtained from the photocatalytic run without bias is also reported. When the applied cell voltage increases from 2 to 3 V, the degradation rate constants of 4-NP increase rapidly from ca. 3×10^{-5} to 19.5×10^{-5} s^{-1}. The degradation of 4-NP was noticeable by applying light and 3 V, with a 4-NP conversion of 70% in 6.5 h of run. These results were expected, since under the applied biases, a potential gradient is established within the titania film, which produced the same effect as band bending in single-crystal photoelectrodes [38]. As the positive potential increases, the resulting gradient separates holes and electrons, decreasing their combination rate, increasing the photocurrent, and eventually accelerating the 4-NP degradation rate.

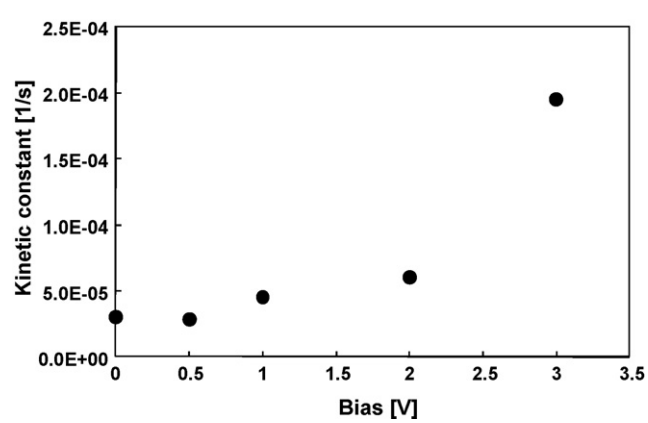

Fig. 10. Kinetic constant, k_T, *vs.* applied bias for photoelectrocatalytic oxidation. 4-NP initial concentration, 7.2×10^{-2} mM; flow rate, 3 mL/s.

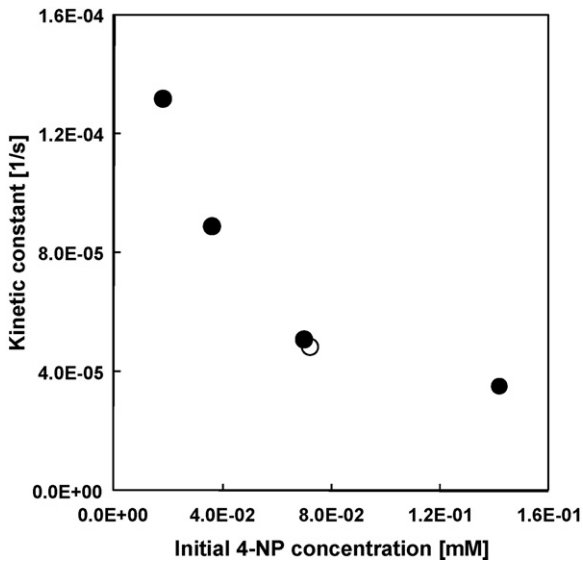

Fig. 11. Kinetic constant, k_T, *vs.* initial 4-NP concentration. The empty symbol refers to a run carried out by using air instead of pure oxygen.

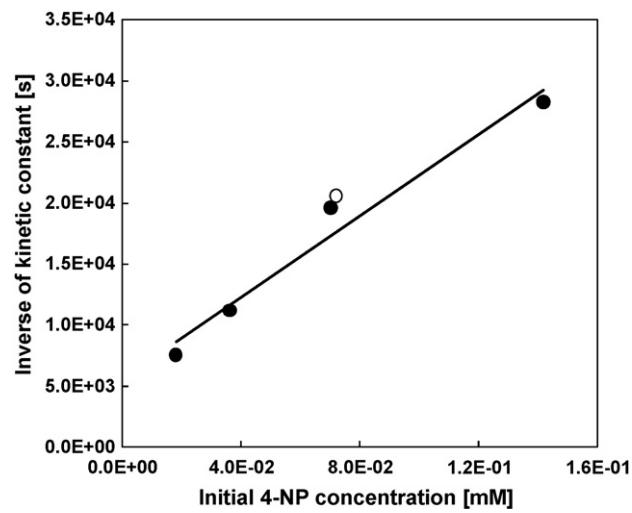

Fig. 12. Linear form of Eq. (8).

Moreover under higher applied cell voltages the external electric field could also improve the direct and/or indirect electro-oxidation reactions at anodes.

3.2.3. *Influence of 4-NP concentration*

Fig. 11 reports the k_T values obtained in photoelectrocatalytic runs (applied potential: +1 V) carried out for investigating the influence of the initial 4-NP concentration on its degradation. This Figure also reports the k_T value obtained in a run carried out at equal reaction conditions but by saturating the electrolyte solution with air instead that with pure oxygen. It may be noted that no appreciable difference in reactivity was found thus indicating that the oxygen concentration does not limit the reaction rate at the used experimental conditions. The k_T values of Fig. 11 indicate that the 4-NP degradation rate decreases as the initial concentration increases. In order to explain this result, it is assumed that the rate-determining step of the 4-NP degradation process is the reaction of organic molecules adsorbed upon the active sites of catalyst surface. These sites are able to adsorb 4-NP and its degradation products. In this hypothesis the reaction rate for the first order surface decomposition of 4-NP may be written in terms of Langmuir–Hinshelwood kinetics as:

$$(-r_{\text{4-NP}}) = k''\theta_{\text{4-NP}} \tag{4}$$

in which k'' is the surface first order rate constant and $\theta_{\text{4-NP}}$ the fractional coverage of the sites by 4-NP molecules. This variable can be written in the following way:

$$\theta_{\text{4-NP}} = \frac{K_{\text{4-NP}}C}{1 + K_{\text{4-NP}}C + \Sigma K_I C_I} \tag{5}$$

in which $K_{\text{4-NP}}$ and K_I are equilibrium adsorption constants of 4-NP and the various intermediate products of 4-NP degradation. Eq. (5), which contains several unknown factors, can be modified by making the following simplifying assumption. Because of the relationship between the adsorption coefficients of 4-NP with its degradation products, it may be assumed that:

$$K_{\text{4-NP}}C + \sum K_I C_I = KC_0 \tag{6}$$

where C_0 is the initial concentration of 4-NP. This is equivalent to assuming that: (i) the adsorption coefficients for the organic molecules present in the reacting mixture are equal; and (ii) the 4-NP degradation does not produce mineralization. By substituting Eq. (6) into Eq. (5), the reaction rate equation becomes:

$$(-r_{\text{4-NP}}) = \frac{k''K}{1 + KC_0}C = k_T C \tag{7}$$

that is a first order kinetic equation with respect to 4-NP concentration. The linear form of k_T is:

$$\frac{1}{k_T} = \frac{1}{k''K} + \frac{1}{k''}C_0 \tag{8}$$

and Fig. 12 reports the $1/k_T$ values versus the C_0 ones. By means of a least-squares best fitting procedure the values of $5.95 \times 10^{-9}\,\text{M}\times\text{s}^{-1}$ and $27.6 \times 10^{3}\,\text{M}^{-1}$ for k'' and K, respectively, have been determined.

4. Conclusion

In conclusion, the easy preparation of new graphite-supported TiO_2 electrodes has been reported. The deposited TiO_2 formed a stable layer and the electrodes were used for 6 months without any drop in reaction rate. A photoelectrochemical reactor, axially irradiated by a near-UV Hg lamp and connected to a potentiostat, was assembled in order to test the prepared catalysts and the reactivity tests indicated that the rods could work as photoanodes in the photoelectrocatalytic oxidation of organic pollutants, such as 4-NP. Applying a small bias of few volts along with light increases the 4-NP oxidation rate so that it may be concluded that 4-NP is more efficiently removed from the wastewater by photoelectrocatalytic process than by individual utilization of either of two other processes, photocatalytic or electrocatalytic.

References

[1] M. Schiavello, Photocatalysis and Environment. Trends and Applications, Kluwer, Dordrecht, 1988.
[2] A.L. Linsebigler, G. Lu, J.T. Yates Jr., Chem. Rev. 95 (1995) 735.
[3] M.R. Hoffmann, S.T. Martin, W. Choi, D.W. Bahnemann, Chem. Rev. 95 (1995) 69.
[4] A. Fujishima, T.N. Rao, D.A. Tryk, J. Photochem. Photobiol. C 1 (2000) 1.
[5] I.M. Butterfield, P.A. Christensen, A. Hamnett, K.E. Shaw, G.M. Walker, S.A. Walker, C.R. Howarth, J. Appl. Electrochem. 27 (1997) 385.
[6] J.M. Kesselman, N.S. Lewis, M.R. Hoffmann, Environ. Sci. Technol. 31 (1997) 2298.
[7] E. Brillas, E. Mur, R. Sauleda, L. Sànchez, J. Peral, X. Domènech, J. Casado, Appl. Catal. B 16 (1998) 31.
[8] R. Pelegrini, P. Peralta-Zamora, A.R. Andrade, J. Reyes, N. Duran, Appl. Catal. B 22 (1999) 83.
[9] R.J. Candal, W.A. Zeltner, M.A. Anderson, Environ. Sci. Technol. 34 (2000) 3443.
[10] X.Z. Li, F.B. Li, C.M. Fan, Y.P. Sun, Water Res. 36 (2002) 2215–2224.

[11] T. An, Y. Xiong, G. Li, C. Zha, X. Zhu, J. Photochem. Photobiol. A 152 (2002) 155.
[12] T. An, X. Zhu, Y. Xiong, Chemosphere 46 (2002) 897.
[13] C. He, Y. Xiong, J. Chen, C. Zha, X. Zhu, J. Photochem. Photobiol. A 157 (2003) 71.
[14] W. Zhang, T. An, X. Xiao, J. Fu, G. Sheng, M. Cui, G. Li, Appl. Catal. A 255 (2003) 221.
[15] V. Subramanian, P.V. Kamat, E.E. Wolf, Ind. Eng. Chem. Res. 42 (2003) 2131–2138.
[16] T. An, W. Zhang, X. Xiao, G. Sheng, J. Fu, X. Zhu, J. Photochem. Photobiol. A 161 (2004) 233.
[17] H. Zhao, D. Jiang, S. Zhang, W. Wen, J. Catal. 250 (2007) 102.
[18] W.H. Leng, Z. Zhang, J.Q. Zhang, J. Mol. Catal. A 206 (2003) 239.
[19] C.-C. Sun, T.-C. Chou, Ind. Eng. Chem. Res. 37 (1998) 4207.
[20] P. Fernandez-Ibañez, S. Malato, O. Enea, Catal. Today 54 (1999) 329.
[21] J.H. Montgomery, L.M. Welkon, Groundwater Chemicals Desk Reference, Lewis Publishers, Chelsea (USA), 1989.
[22] V. Augugliaro, M.J. López, L. Palmisano, J. Soria, Appl. Catal. A. 101 (1993) 7.
[23] M. Addamo, V. Augugliaro, A. Di Paola, E. García-López, V. Loddo, G. Marcì, R. Molinari, L. Palmisano, M. Schiavello, J. Phys. Chem. B 108 (2004) 3303.
[24] S. Yurdakal, V. Loddo, G. Palmisano, V. Augugliaro, H. Berber, L. Palmisano, J. Adv. Oxid. Technol. 11 (2008) 501.
[25] P. Piccinini, C. Minero, M. Vincenti, E. Pelizzetti, J. Chem. Soc. Faraday Trans. 93 (1997) 1993.
[26] A. Di Paola, V. Augugliaro, L. Palmisano, G. Pantaleo, E. Savinov, J. Photochem. Photobiol. A 155 (2003) 207.
[27] M.A. Quiroz, S. Reyna, C.A. Martínez-Huitle, S. Ferro, A. De Battisti, Appl. Catal. B 59 (2005) 259.
[28] Q. Dai, L. Lei, X. Zhang, Sep. Purif. Technol. 61 (2008) 123.
[29] S.M. Alves Jorge, J.J. de Sene, A. de Oliveira Florentino, J. Photochem. Photobiol. A 174 (2005) 71.
[30] T.A. Egerton, P.A. Christensen, S.A.M. Kosa, B. Onoka, J.C. Harper, J.R. Tinlin, Int. J. Env. Poll. 27 (2006) 2.
[31] B. Su, Y. Ma, Y. Du, C. Wang, Electrochem. Comm. 11 (2009) 1154.
[32] K.L. Yeung, A.J. Maira, J. Stolz, E. Hung, N.K.C. Ho, A.C. Wei, J. Soria, K.J. Chao, J. Phys. Chem. B 106 (2006) 4608.
[33] K.L. Yeung, W.K. Leung, N. Yao, S.L. Cao, Catal. Today 143 (2009) 218.
[34] S.L. Cao, K.L. Yeung, J.K.C. Kwan, P.M.T. To, S.C.T. Yu, Appl. Catal. B 86 (2009) 127.
[35] X.-M. Song, J.-M. Wu, M. Yan, Mat. Chem. Phys. 112 (2008) 510.
[36] K. Nagaveni, G. Sivalingam, M.S. Hedge, G. Madras, Appl. Catal. B 48 (2004) 83.
[37] E.J. Wolfrum, C.G. Turchi, J. Catal. 136 (1992) 626.
[38] K. Vinodgopal, S. Hotchandani, P.V. Kamat, J. Phys. Chem. 97 (1993) 9040.